



I S A V

Journal of Theoretical and Applied
Vibration and Acoustics

journal homepage: <http://tava.isav.ir>



Studying free vibration of tympanic membrane using analytical, finite element and Rayleigh-ritz approaches

M. Mohammad-Reza Ommatmohammadi ^a, Hadi Majdi ^a,
Jafar Keighobadi ^{a,*}

^a Department of Mechanical Engineering, University of Tabriz, Tabriz, Iran

Research Article

ARTICLE INFO

Article history:

Received 10 February 2025

Received in revised form
22 August 2025

Accepted 30 August 2025

Available online 3 November 2025

Keywords:

Tympanic membrane

Natural frequency acoustics

Mode shapes

Rayleigh-Ritz method

Parameter variation

ABSTRACT

The tympanic membrane TM plays a central role in the human hearing mechanism. Located at the entrance to the middle ear, it vibrates in response to changes in air pressure generated by incoming sound waves. The oscillation characteristics—particularly the natural frequencies and associated mode shapes—directly influence auditory perception and hearing sensitivity. This study investigates the TM's natural frequencies using a simplified yet representative mathematical model, employing both analytical and semi-analytical approaches. The semi-analytical analysis is conducted using the Rayleigh–Ritz method with various basis functions to assess their accuracy in predicting frequency and mode shapes. Among these, Chebyshev polynomials exhibit exceptional efficiency, yielding high-accuracy frequency estimates in close agreement with analytical solutions and validated by finite-element simulations. In addition, the study examines the sensitivity of TM modes to variations in geometric and material parameters, providing valuable insight into their influence on dynamic behavior. A comparative analysis confirms that Chebyshev polynomials deliver the most accurate results, outperforming the other basis functions considered.

© 2025 Iranian Society of Acoustics and Vibration, All rights reserved.

* Corresponding author.

E-mail address: keighobadi@tabrizu.ac.ir (J. keighobadi)

1. Introduction

Membranes are perfectly flexible, thin structures subjected to tensile forces, offering negligible resistance to bending or shear. Their restoring forces originate solely from in-plane stretching or pretension [1]. They have diverse engineering applications: airbag deployment systems use membranes to trigger inflation during collisions, while reverse osmosis relies on them for water purification [2-4]. Vibrating membranes are critical in devices like speakers, where membrane movement converts electrical signals into sound waves, and pressure sensors, where pressure-induced deformation alters vibration characteristics for measurement [5-7]. They are also fundamental in ultrasonic applications—including medical imaging, fingerprint recognition, and nondestructive testing—where membranes generate and detect ultrasonic waves via specific-frequency vibrations [4, 8-11]. Hence, understanding membrane vibration behavior and the influence of parameters is essential for the design of these systems.

Membranes extend beyond artificial structures; the human body contains vital biological membranes, such as cell and synovial membranes, each of which performs numerous functions [12, 13]. Among these, the tympanic membrane (TM), or eardrum, is critically important. Located at the entrance to the middle ear, the TM vibrates in response to changes in air pressure induced by sound. Three ossicles—the malleus, incus, and stapes—amplify these vibrations and transmit them to the cochlea within the inner ear. This spiral-shaped structure contains hair cells that convert mechanical vibrations into neural signals for the auditory nerve. Since the story of hearing begins with the vibration of the TM, studying its displacement characteristics experimentally, mathematically, or via simulation is essential. This work first surveys key studies of the TM from a mechanical engineering analysis perspective. We then investigate common mathematical approaches used by researchers in vibration analysis, particularly semi-analytical methods.

Yao et al. [14] developed a finite element model based on clinical CT images. This model simulates the left and right inner boundaries of the middle ear and accounts for the coupling between the gas in the external ear canal and the eardrum. This approach better reflects the sound-pressure stimulation transmitted from the external canal to the middle ear. The proposed model captures sound transmission behavior through the interaction of the outer, middle, and inner ear. Ugarteburu et al. [15] reviewed mammalian middle ear mechanics, suggesting the TM's form may explain mammals' broader hearing range compared to other terrestrial vertebrates. Reported TM stiffness values varied significantly (2.1 to 300 MPa), even with identical testing methods. This variation stems from differences in testing methodologies, specimen preparation, inter-specimen variability, TM heterogeneity, and tissue sample locations.

Caminos et al. [16] examined two key parameters defining TM bending stiffness: Young's modulus and thickness. They demonstrated that while membrane parameter changes minimally affect lower natural frequencies, thickness, elastic modulus, and pre-strain significantly impact higher natural

frequencies. Wu et al. [17] modeled the eardrum as a sectorial annulus incapable of resisting shear deformation or bending, with horizontal load balance reliant solely on annular ligament tension. Their results identified material stiffness, thickness, curvature, conical shape, and anisotropy as critical determinants of low-frequency TM behavior. At the same time, boundary conditions, Poisson's ratio, ossicular loading, and air loading were less significant. In a separate study, Wu et al. [18] modeled the TM as a plate, finding that diameter and thickness variations caused natural frequency errors exceeding 40%, whereas Young's modulus and density induced errors below 15%. Natural frequencies were obtained via separation of variables. Lobato et al. [19] gathered and reevaluated experimental data on middle-ear mechanical properties to assess uncertainty and establish a foundation for probabilistic middle-ear models. Zhang and Gan [20] emphasized the TM's dynamic properties, which directly influence the middle ear's sound transmission. Their results indicate that frequency-temperature superposition is a viable approach for studying ear soft-tissue dynamics. The obtained TM properties provide a better description of ear tissue damping behavior. The frequency-temperature superposition principle using a Dynamic Mechanical Analyzer offers a potential method for measuring TM dynamic properties across the auditory frequency range.

Mathematical methods, particularly analytical and semi-analytical approaches, are widely employed for vibration analysis across engineering disciplines. Among these, the Rayleigh-Ritz method is a pivotal semi-analytical technique for solving eigenvalue problems derived from physical boundary value problems. Its versatility spans vibration studies of structures ranging from simple to geometrically complex configurations.

Ahmadvand and Asadi [21] employed the Rayleigh-Ritz method to examine the natural oscillations of a three-dimensional tank, with four flexible walls and a surface crack. The shape of the function is determined by a set of differential equations that describe the behavior of horizontal and vertical static beams. Mochida and Ilanko [22] applied three techniques, including the Rayleigh-Ritz method, Gorman's superposition approach, and the exact dynamic stiffness method, to analyze the vibration and stability of continuous systems. They then examined the advantages and most suitable applications of each technique. Ye and Wang [23] used the Kirchhoff-Love shell theory to derive a mathematical model of cylindrical shells composed of three-dimensional graphene foam. They then computed the buckling load and natural frequency using the Rayleigh-Ritz method, whose shape functions are Chebyshev polynomials. The Rayleigh-Ritz method was employed by Du et al. [24] to investigate the free vibration of rotating cylindrical casings with hard coatings in various boundary conditions. The admissible displacement functions were the characteristic orthogonal polynomials. Bao et al. [25] investigated the free vibration of nanorods along the longitudinal axis. Auxiliary trigonometric functions and the Fourier series are thought to combine linearly to explain the longitudinal displacement of nanorods. The Rayleigh-Ritz method is used to obtain the coefficients of the improved Fourier series expansion for the displacements. Njim et al. [26] proposed a new approximated analytical solution based on classical plate theory.

They used the Rayleigh-Ritz approach to determine natural frequencies based on various parameters. Hussain et al. [27] employed Sander's shell theory and the Rayleigh-Ritz method, incorporating Hankel's function, to explore the vibration characteristics of fluid-filled, functionally graded cylindrical shells.

Few scientific papers have examined the accuracy and performance of semi-analytical methods for approximating the dynamic behavior of membranes. This work uses the Rayleigh-Ritz method with different basis functions, including Chebyshev polynomials, to determine the natural frequencies of TM. We compare the extracted results with the analytical solution to illustrate the power of each basis function. On the other hand, we investigate the dependence of the membrane's natural frequencies on model parameters to determine the impact of each parameter variation on the natural frequencies.

2. Material and methods: Mathematical formulation (Methodology)

This study presents a mathematical analysis of the free vibration of the human eardrum. Hence, precise specification of the geometry, physical properties, material parameters, and governing equation of motion is essential. As established in prior research [17], we model the eardrum as a thin membrane—a common and validated assumption in biomechanics. The equation of motion is therefore expressed as follows [1]:

$$\nabla^2 w + \frac{\tau}{\sigma} = \frac{1}{c^2} \frac{\partial^2 w}{\partial t^2}$$

$$c = \sqrt{\frac{\sigma}{\rho}}$$
(1)

In this context, the symbol ∇^2 denotes the Laplacian operator, w represents the out-of-plane deformation field, and c is the wave propagation speed, σ denotes the radial pretension applied to the membrane. In contrast, τ signifies the external excitation—present only in forced vibrations—which may vary spatially and temporally.

2.1. Model description

Given the annular geometry presented in Figure 1, it is mathematically advantageous to express the governing differential equation in polar coordinates. Transforming the Laplacian operator from Cartesian to polar coordinates yields the following equation for membrane free vibrations [1]:

$$\nabla^2 w(r, \theta) = w_{rr} + \frac{w_r}{r} + \frac{w_{\theta\theta}}{r^2} = \frac{1}{c^2} \frac{\partial^2 w}{\partial t^2}$$

$$\begin{aligned} 0 &\leq t \\ R_1 &\leq r \leq R_2 \\ \alpha &\leq \theta \leq 2\pi \end{aligned}$$
(2)

Table 1 presents the geometrical parameters and mechanical properties of the considered model. Since Eq. (2) includes partial derivatives with respect to r , θ , and t , it is necessary to introduce

some Boundary Conditions (B.Cs) and some Initial Conditions (I.Cs) to achieve a unique response for the problem. All boundaries are assumed to be clamped. Thus, the B.Cs are stated as:

$$\begin{aligned} w(R_1, \theta, t) = 0 & \quad , & w(R_2, \theta, t) = 0 \\ w(r, \alpha, t) = 0 & \quad , & w(r, 2\pi, t) = 0 \end{aligned} \quad (3)$$

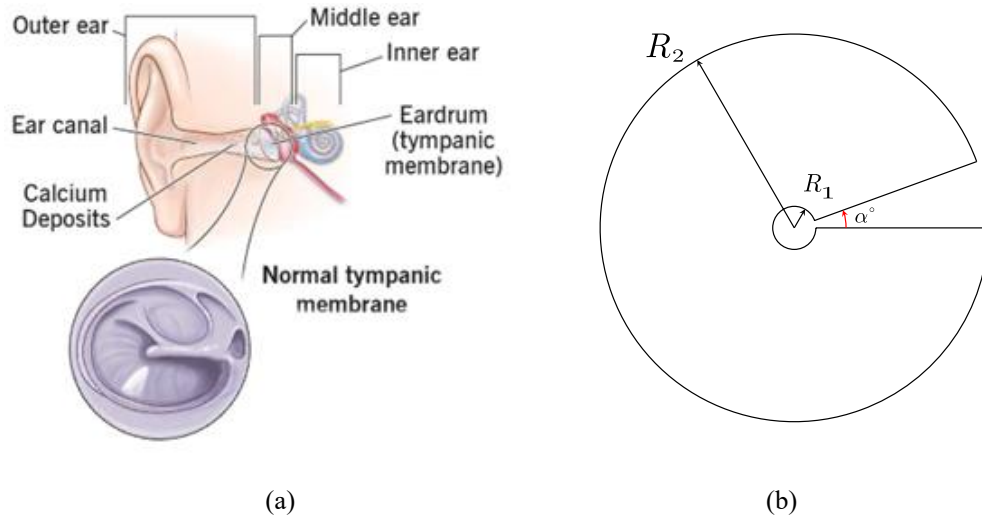


Fig. 1. (a) Real image of the human tympanic membrane, and (b) Geometry of the model. [28]

Table 1. Model characteristics [17].

Symbol	Description	value
R_1	Inner radius of circle	0.5 mm
R_2	Inner radius of circle	4.5 mm
α	Outer radius of circle	20 deg
ρ	Angle of empty section	1200 kg/m ³
σ	Material density	35 kPa
c	Membrane pretension	5.4 m/sec

2.2 Analytical natural frequencies of TM

The separation of variables method can be applied to Eq. (2), as both the equation and the B.C. are linear and homogeneous. Firstly, the separation should differentiate time from space:

$$w(r, \theta, t) = u(r, \theta) q(t) \quad (4)$$

hence,

$$\frac{\nabla^2 u(r, \theta)}{u} = \frac{1}{c^2} \frac{\ddot{q}(t)}{q} = -\lambda^2 < 0 \quad (5)$$

The left-hand side of Eq. (5) depends solely on spatial coordinates, while the right-hand side is exclusively time-dependent. For this equality to hold, both sides must equal a *negative constant to satisfy the separation of variables*. This constraint ensures oscillatory solutions in time. Consequently, we express the temporal component as:

$$q(t) = q_0 \sin(\omega t + \psi) = q_0 \sin(c\lambda t + \psi) \quad (6)$$

where $\omega = c\lambda$ is the frequency of vibration, and both of the q_0 will be determined using I.Cs. The solution in the space domain is separated and given as

$$u(r, \theta) = H(r) G(\theta) \quad (7)$$

hence,

$$r^2 \frac{H''}{H} + r \frac{H'}{H} + \lambda^2 r^2 = -\frac{G''}{G} = n^2 \geq 0 \quad (8)$$

The left-hand side of Eq. (8) depends exclusively on the radial coordinate r , while the right-hand side depends solely on the angular coordinate θ . For this equality to hold, both sides must equal a *non-negative constant n^2* (where n is an integer). This constraint is necessary to satisfy the periodic boundary conditions required for annular domains. Rewriting Eq. (8) leads us to two sets of ordinary differential equations; one is for $n > 0$ and the other is for $n = 0$:

$$r^2 H'' + r H' + (\lambda^2 r^2 - n^2) H = 0 \quad \text{for } n > 0 \quad (9)$$

$$G'' + n^2G = 0 \quad \text{for } n = 0 \quad (10)$$

Eq. (9) represents the classical Bessel differential equation, whose solutions are the Bessel functions, and Eq. (10) is a simple equation that is satisfied by sine and cosine functions or a linear function:

$$H(r) = h_1 J_n(\lambda r) + h_2 Y_n(\lambda r) \quad (11)$$

$$G(\theta) = g_1 \sin(n\theta) + g_2 \cos(n\theta) \quad n > 0 \quad (12-1)$$

$$G(\theta) = g_3\theta + g_4 \quad n = 0 \quad (12-2)$$

The functions J_n and Y_n are named as first and second kind Bessel functions of order n , respectively. The boundary conditions must be used to compute all constant coefficients (h_i and g_i). Separation of variables yields two distinct cases for the angular eigenvalue: $n = 0$ (axisymmetric modes) and $n > 0$. For $n=0$, enforcement of the boundary conditions produces only trivial solutions. This scenario arises because sectorial membranes lack closed rotational symmetry, rendering axisymmetric modes mathematically inadmissible. Consequently, for non-circular geometries, we exclusively consider $n \geq 1$. The physically meaningful solution is therefore given by Eq. (12-1), with non-trivial modes satisfying the following equations:

$$n = \frac{\pi}{2\pi - \alpha} k \quad k \in \mathbb{N} \quad , \quad \frac{g_2}{g_1} = -\tan n\alpha \quad , \quad \frac{h_2}{h_1} = -\frac{J_n(\lambda R_2)}{Y_n(\lambda R_2)} \quad (13)$$

$$\begin{vmatrix} J_n(\lambda R_1) & Y_n(\lambda R_1) \\ J_n(\lambda R_2) & Y_n(\lambda R_2) \end{vmatrix} = 0 \quad (14)$$

For each value of k , we can find numerous answers for λ , since Bessel functions have innumerable zeros. By multiplying λ by c as described in Eq. (6), the natural frequencies of the membrane are obtained:

$$\omega_m^k = 2\pi f_m^k = c\lambda_m^k \quad (15)$$

where m is the m -th answer resulting from Eq. (14) and f_m^k is the corresponding natural frequency in Hz. In a non-dimensional form, the natural frequencies are derived from this equation:

$$J_{\frac{k\pi}{2\pi-\alpha}}(\Omega_m^k) Y_{\frac{k\pi}{2\pi-\alpha}}(r' \Omega_m^k) = J_{\frac{k\pi}{2\pi-\alpha}}(r' \Omega_m^k) Y_{\frac{k\pi}{2\pi-\alpha}}(\Omega_m^k) \quad (16)$$

where r' is the radius ratio and Ω_m^k is the dimensionless frequency, defined as:

$$r' = \frac{R_2}{R_1} \quad (17)$$

$$\Omega_m^k = \lambda_m^k R_1 = \frac{\omega_m^k}{c} R_1 = \frac{2\pi f_m^k}{c} R_1 \quad (18)$$

For certain boundary conditions, the dimensionless frequency (Ω_m^k) is dependent on the empty section angle (α) and radius ratio (r'). Therefore, it is independent of material density (ρ) and pretension (σ).

2.3. Natural frequencies of TM using the Rayleigh-Ritz method

Mathematically modeling vibrating membranes, such as the tympanic membrane (TM), requires partial differential equations (PDEs) to describe their continuous behavior. Key factors influencing vibrations include geometry, material properties, tensile pretension, excitation characteristics, and boundary/initial conditions. Free vibration analysis yields natural frequencies (eigenvalues) and mode shapes (eigenfunctions). When analytical PDE solutions are intractable due to complex boundaries or materials, semi-analytical methods offer an alternative. These methods approximate the solution as a series expansion, with basis functions spanning the spatial domain chosen to satisfy the PDE and boundary conditions—either *exactly* (strong form) or *approximately* (weak form). Orthogonal bases are often preferred due to completeness.

One of the most famous semi-analytical techniques in structural analysis, particularly in buckling and vibration problems, is the Rayleigh-Ritz method. This method uses a linear combination of a set of complete functions as analytical mode shapes that satisfy the boundary conditions. Depending on whether the mentioned functions satisfy both natural and geometric boundary conditions or only the geometric boundary conditions, they are referred to as comparison or admissible functions, respectively. The coefficients of these functions are determined by minimizing a ratio called Rayleigh's quotient, whose numerator and denominator are expressed as the maximum strain energy (E_p) and maximum reference kinetic energy (E_k^*) of the system, respectively [1]. This minimization results in an eigenvalue problem in which the eigenvalues are the squared natural frequencies and the eigenvectors are the coefficients, making the assumed mode functions physically meaningful. For a membrane structure in polar coordinates, the energies can be calculated as follows:

$$E_p(t) = \frac{\sigma}{2} \iint [(\frac{\partial w}{\partial r})^2 + (\frac{1}{r} \frac{\partial w}{\partial \theta})^2] r dr d\theta \quad (19-1)$$

$$E_k^*(t) = \frac{\rho h}{2} \iint w^2 r dr d\theta \quad (19-2)$$

The deformation field, w , is approximated with the sum of admissible functions $\hat{u}_{i,j}$ multiplied by coefficients $v_{i,j}$ and the corresponding generalized coordinate $q_{i,j}$ as stated below:

$$w(r, \theta, t) \cong \sum_{i=1}^{M'} \sum_{j=1}^{N'} (\hat{u}_{i,j}(r, \theta) v_{i,j}) q_{i,j}(t) \quad (20)$$

This substitution converts the continuous system to a discrete one with $M' \times N'$ degrees of freedom. Thus, the stiffness K and mass M matrices are represented as follows:

$$\max (E_p) = \frac{1}{2} v^T K v \rightarrow K(l, p) = \frac{\partial^2 E_p}{\partial v_l \partial v_p} \quad (21-1)$$

$$\max (E_k^*) = \frac{1}{2} v^T M v \rightarrow M(l, p) = \frac{\partial^2 E_k^*}{\partial v_l \partial v_p} \quad (21-2)$$

$$1 \leq l, p \leq M' \times N'$$

The natural frequencies are derived from the eigenvalue problem in the following form:

$$[K]\{v\} = \omega^2 [M]\{v\} \quad (22)$$

The values of ω^2 are the eigenvalues, and the vectors v are the eigenvectors. Physically, ω is the natural frequency, and $v * u$ is the mode shape corresponding to ω .

3. Results and discussion

This section presents the analytical solution and the frequency trend with respect to the root number (m) and the Bessel counter (n) for different parameter variations, followed by an examination of the accuracy of the Rayleigh-Ritz method for varying basis functions. A finite

element approach is also used for validation. Finally, the dependence of the natural frequencies on different parameters in the membrane model will be studied.

3.1 Analytical approach

According to the methodology presented in section 2, the natural frequency in certain boundary conditions has a functionality as follows:

$$f_m^k = c F(\alpha, R_1, R_2) = \sqrt{\frac{\sigma}{\rho}} F(\alpha, R_1, R_2) \quad (23)$$

Based on the parameter values in Table 1, the analytical natural frequencies are illustrated in the contour plot of Figure 2. Assuming ascending order, the frequencies can be written using a single index, f_n . Hence, f_1 will correspond to the fundamental frequency f_1^1 .

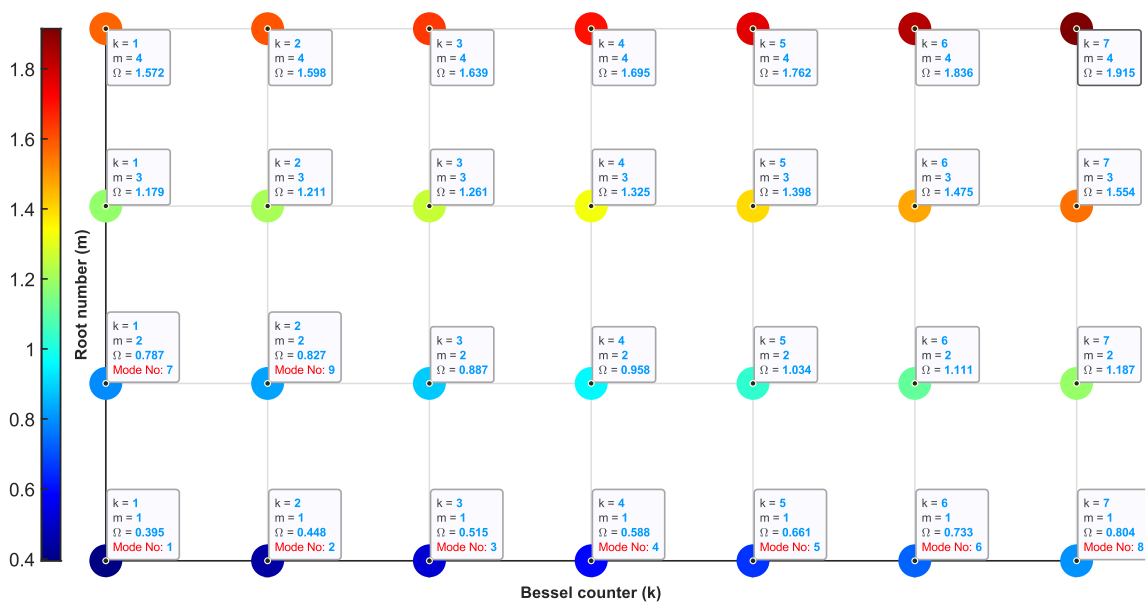


Fig. 2. Dimensionless natural frequencies derived from analytical solution

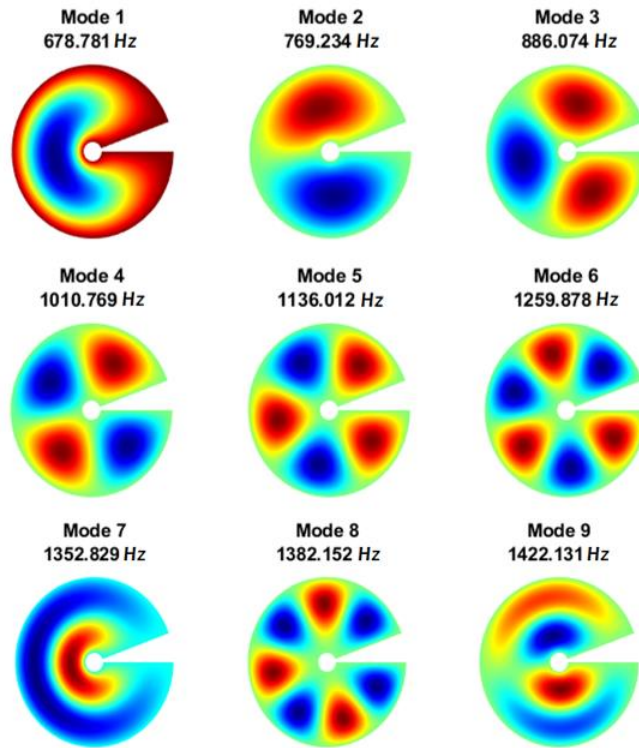


Fig. 3. Analytical mode shapes of TM with corresponding frequency

The following can be concluded from the results shown in Figures 2 and 3:

1- Greater "m" corresponds to a greater frequency when the geometrical and mechanical characteristics and a given Bessel number remain constant. The radial axis shows the mode's ups and downs as a function of the root number (m). As frequency rises, so will the total number of ups and downs.

2- A greater "k" corresponds to a greater frequency when the geometrical and mechanical characteristics and the given root number "m" remain constant. The angular axis shows the ups and downs of the mode as a function of "k". As the frequency increases, so does the total number of ups and downs.

3- More intensity is found in the frequency gradient along the root number "m" than along the Bessel counter "k."

3.2. Natural frequencies by Rayleigh-Ritz method

Three different functions are considered as basis mode functions of the displacement, w :

$$P_1(r, \theta) = \sum_{i=0}^I \sum_{j=0}^J (r - R_1)(r - R_2)(\theta - \alpha)(\theta - 2\pi) r^i \theta^j \quad I = 2, J = 7 \quad (24-1)$$

$$P_2(r, \theta) = \sum_{i=0}^I \sum_{j=1}^J (r - R_1)(r - R_2) r^i \sin\left(j\pi \frac{\theta - \alpha}{2\pi - \alpha}\right) \quad I = 2, J = 8 \quad (24-2)$$

$$P_3(r, \theta) = \sum_{i=0}^I \sum_{j=1}^J (r - R_1)(r - R_2) T_i(r) \sin\left(j\pi \frac{\theta - \alpha}{2\pi - \alpha}\right) \quad I = 3, J = 8 \quad (24-3)$$

where $T_i(r)$ denotes the first kind of Chebyshev polynomials. Each upper bound of the summation is chosen to encompass all nine aforementioned analytical frequencies and to keep computational cost low. These functions $\hat{u}(r, \theta)$ serve a specific purpose in Eq. (20). The error percentage (%e) is considered as a criterion to evaluate the accuracy of each approximation, calculated from the following formula:

$$\%e = \frac{f_{\text{approx}} - f_{\text{analytic}}}{f_{\text{analytic}}} \times 100 \quad (1)$$

Chebyshev polynomials clearly demonstrate their ability to estimate frequency with significant accuracy, as shown in Figure 3. To provide more clarification, approximated mode shapes of Chebyshev polynomials are shown in Figure 4. As shown, the Chebyshev polynomials not only achieve high accuracy in estimating higher-frequency natural frequencies but also approximate the shapes of analytical modes well, as demonstrated in Figure 5.

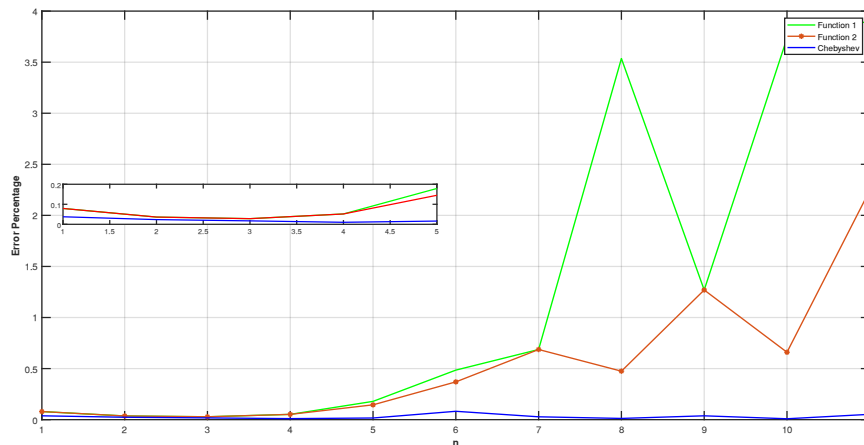


Fig.4. Percentage error in the natural frequencies for the first eleven modes, ordered from the lowest to highest frequency, comparing P_1 , P_2 , and P_3 w.r.t analytical ones (%e)

3.3. Validation with Finite Element Analysis

In addition to the analytical and semi-analytical approaches described earlier, a numerical simulation of the tympanic membrane was performed in COMSOL Multiphysics 6.2 for validation. The membrane geometry and material parameters were modeled according to Table 1, and the boundary conditions corresponded to the clamped configuration used in the theoretical analysis. The Solid Mechanics physics interface was employed, with eigenfrequency analysis conducted to extract the first six natural frequencies. A finite element mesh was generated using free triangular elements to discretize the computational domain (see Figure 6). The mesh characteristics are as follows:

- Element type: Free triangles
- Number of elements: 721
- Average quality (skewness): 0.84

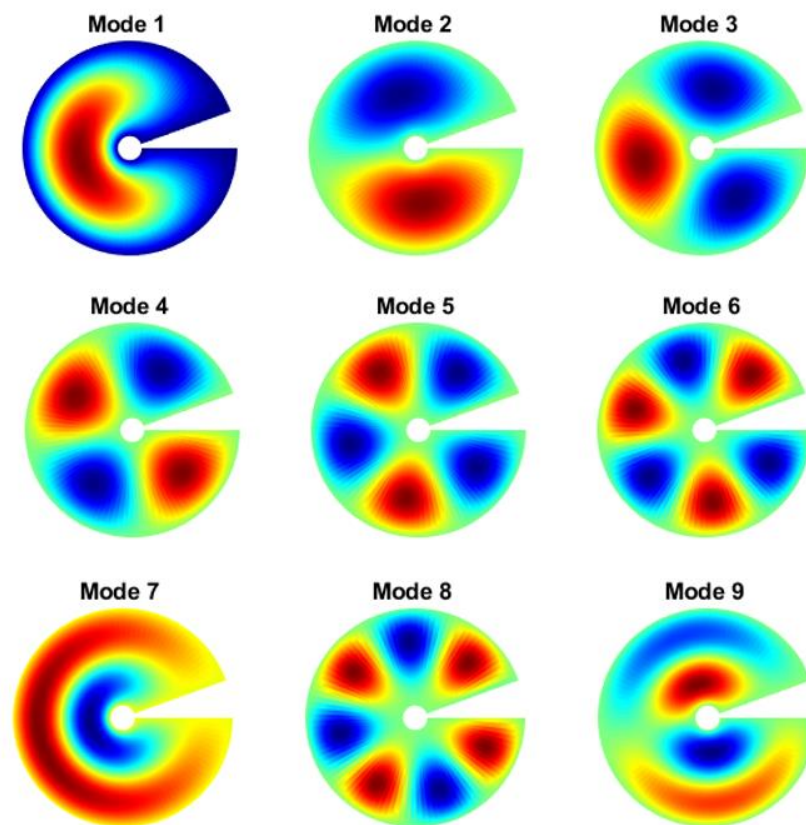


Fig. 5. Rayleigh-Ritz mode shapes using Chebyshev polynomials

The mesh quality was sufficient to ensure convergence and accuracy for the studied modes, and refinement was continued until no significant change in computed frequencies was observed. The

first nine modes obtained from the COMSOL simulation are summarized in Figure 7, and the frequencies are given in Table 2. These frequencies show excellent agreement with both the analytical solution and the semi-analytical Rayleigh-Ritz estimates, thereby confirming the validity of the Chebyshev-polynomial-based approach across multiple computational methods.

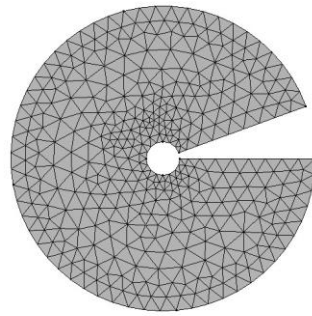


Fig. 6. Mesh structure of FEM simulation

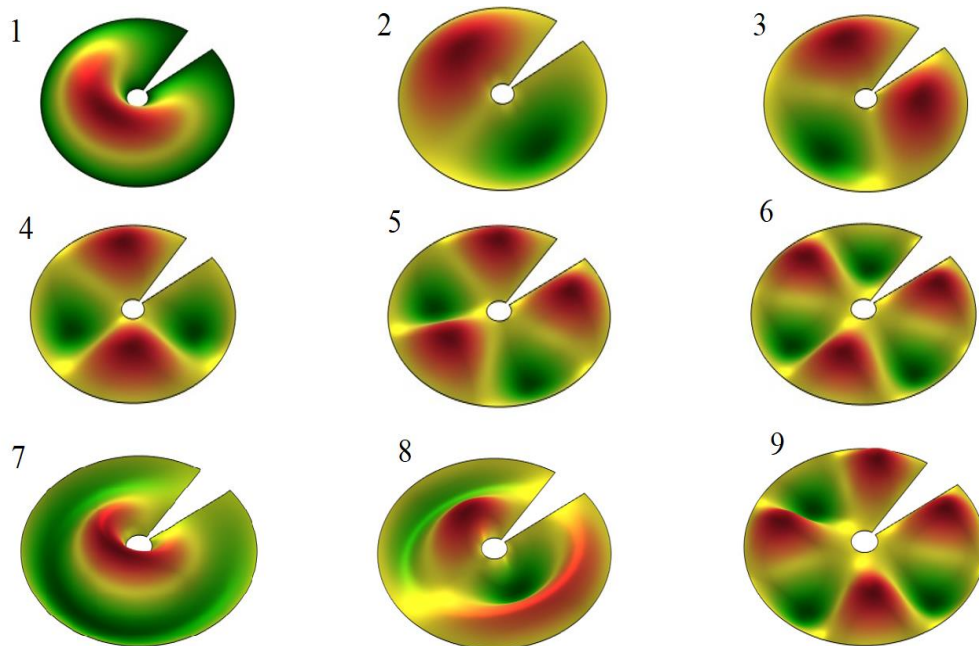


Fig.7. Computational results for mode shapes (1 to 9) derived from the FEM method

Table 2. Comparison between different methods of calculating natural frequencies (Hz).

Mode No.	Analytical	FEM by COMSOL	Rayleigh-Ritz with P ₃
1	678.78	678.8	679.0055
2	769.23	769.3	769.3906
3	886.07	886.1	886.2083
4	1010.77	1010.8	1010.902
5	1136.01	1136.1	1136.184
6	1259.88	1260.0	1260.03
7	1352.83	1353.0	1353.377
8	1382.15	1382.4	1382.234
9	1422.13	1422.3	1422.834

3.4. Effect of model parameters on natural frequency

For a more profound understanding of how different parameters affect the natural frequency, the trend of frequency behavior along two indices, ‘m’ and ‘k’, was investigated. Given the linear dependence of (ω_m^k) on wave propagation speed is linear, on the wave propagation speed, its trend with respect to density and pretension follows directly from Eq. (23). Thus, only the variation of radius and the empty section angle will be analyzed. To visualize the results in 2D plots, the characteristic equation for the dimensionless frequency, Eq. (16), is used for analysis. The parameters are varied around the values introduced in Table 1. In Figure 6, the empty section angle is assumed to be constant ($\alpha = 20^\circ$), and in Figure 7, the radius ratio ($r' = 9$) is assumed to be constant.

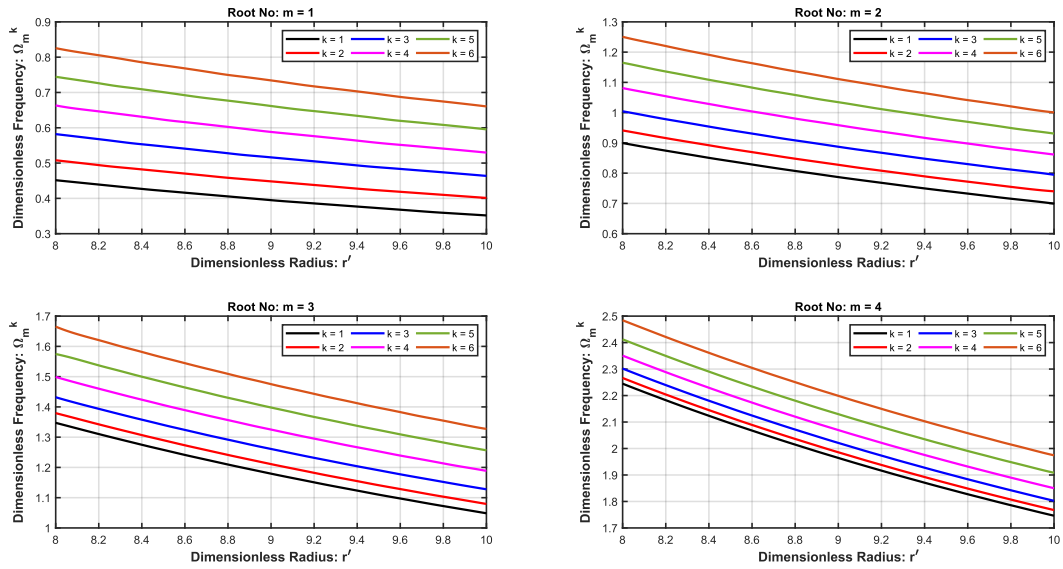


Fig. 8. Dimensionless frequency trend with respect to variation of dimensionless radius

A conclusion can be drawn based on the presented evidence:

- As the radius ratio increases, the dimensionless frequency decreases.
- Variation of dimensionless frequency with respect to radius ratio increases with the increase of ‘m’.
- Variation of the dimensionless frequency with respect to the radius ratio, for different k values, behaves similarly.

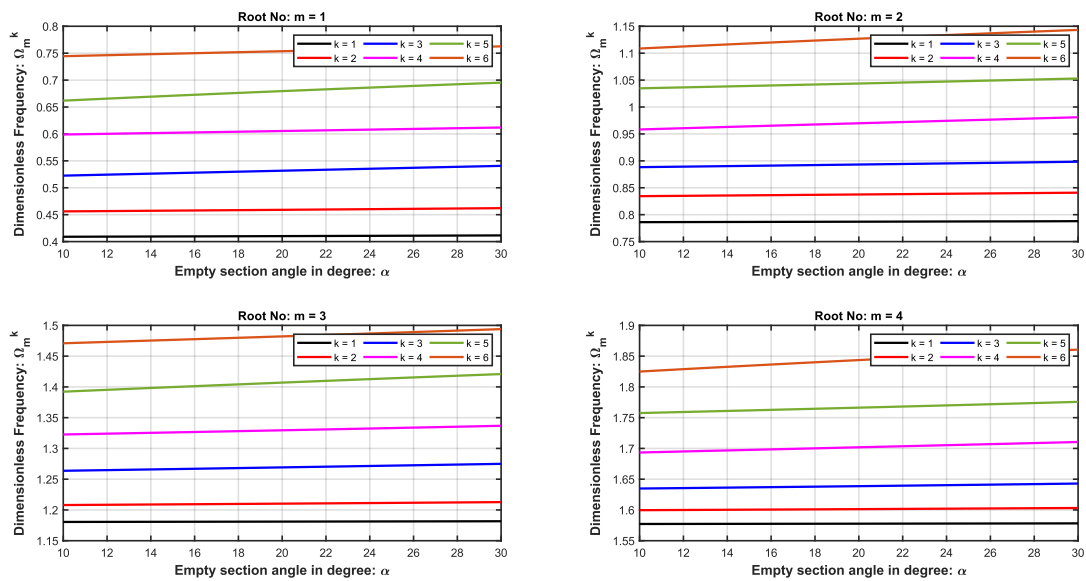


Fig. 9. Dimensionless frequency trend with respect to variation of empty section angle

The following can be inferred from varying values of alpha:

- Variation of dimensionless frequency with respect to alpha angle increases slightly with increasing k value.
- The variation of the dimensionless frequency with respect to alpha is similar for various values of m.

3.5. Limitations of the present model

Complex anatomical and material features of the tympanic membrane in vivo include its conical curvature, anisotropic fiber arrangement, spatially variable thickness, and mechanical coupling to neighboring middle ear structures. The TM was idealized in the current formulation as a homogeneous, flat, isotropic membrane of constant thickness, subjected to uniform in-plane pretension. Although such an ideal is a typical and useful assumption in vibration modeling, it inevitably ignores the directional stiffness that is provided by the networks of collagen fibers that run radially and circumferentially, as well as any thickness gradient, all of which can affect mode shapes and higher-order frequencies. With all boundaries assumed to be perfectly clamped, the geometry was further reduced to a sectorial annulus with an empty sector of alpha, an inner radius R_1 , and an outer radius R_2 . Additionally, the potential mechanical impacts of viscoelastic damping and partial ossicular attachment were disregarded. At high frequencies, anisotropy, curvature, and coupled fluid–structure effects become more pronounced, and these simplifications limit direct quantitative comparisons with in vivo measurements. This model is therefore the most appropriate for qualitatively analyzing parameter sensitivity, evaluating basis functions comparatively, and observing trends in modal behavior under controlled variations of geometry and pretension.

4. Conclusion

In the present study, we employed the Rayleigh-Ritz method to investigate the free vibration characteristics of the tympanic membrane, a crucial component of the human auditory system. By utilizing different basis functions, including Chebyshev polynomials that approximate the natural frequencies with amazing accuracy, we demonstrated the effectiveness of this semi-analytical approach for computing the natural frequencies of the TM. Furthermore, another analysis was conducted to examine the impact of various model parameters on the TM's natural frequencies. The results showed that an increase in the radius ratio decreases the dimensionless frequency dramatically, while an increase in the empty section angle increases the dimensionless frequency negligibly. This comprehensive analysis provides detailed insights into the TM's dynamic behavior and its potential implications for human hearing. The findings of this study can contribute to a deeper understanding of the auditory system and inform the development of more effective treatments for hearing-related disorders.

Reference

- [1] S.S. Rao, *Vibration of continuous systems*, John Wiley & Sons, 2019.
- [2] S. Satapathy, S. Sahu, S. Roychowdhury, Impact of a spherical body on an air-inflated membrane structure, *Thin-Walled Structures*, Vol. 191,(2023)
- [3] E.A. Al-Bahkali, H. Elkenani, M. Souli, F. Erchiqui, M. Moatammed, "Investigation of particle method and FEM coupling method for automotive airbag," in *Multiphysics Simulations in Automotive and Aerospace Applications*: Elsevier, 2021, pp. 1-20.
- [4] R.H. Hailemariam, Y.C. Woo, M.M. Damtie, B.C. Kim, K.D. Park, J.S. Choi, Reverse osmosis membrane fabrication and modification technologies and future trends: A review, *Advances in Colloid and Interface Science*, Vol. 276,(2020)
- [5] S. Naserbakht, A. Dantan, Squeeze film pressure sensors based on SiN membrane sandwiches, *Sensors and Actuators A: Physical*, Vol. 298,(2019)
- [6] T. Liu, et al., Facilely prepared layer-by-layer graphene membrane-based pressure sensor with high sensitivity and stability for smart wearable devices, *Journal of Materials Science & Technology*, Vol. 45,(2020)
- [7] Z. Mehmood, I. Haneef, F. Udrea, Material selection for optimum design of MEMS pressure sensors, *Microsystem Technologies*, Vol. 26, Iss.9,(2020)
- [8] U. Kumar, S.N.S. Dontaraju, S. Sinha, Design, Modelling, and Simulation of PMUT Device for Ultrasound Imaging Applications, in *2023 16th International Conference on Sensing Technology (ICST)*, 2023: IEEE, pp. 1-6.
- [9] Z. Wang, et al., Investigation of Submerged MEMS Ultrasonic Sensors for Underwater Obstacle Avoidance Application, *Remote Sensing*, Vol. 16, Iss.3,(2024)
- [10] P. Li, et al., Enhancement of the transmission performance of piezoelectric micromachined ultrasound transducers by vibration mode optimization, *Micromachines*, Vol. 13, Iss.4,(2022)
- [11] R. Zhang, Y. Huang, C. Sun, L. Xiaozhen, X. Bentian, Z. Wang, Study on ultrasonic techniques for enhancing the separation process of membrane, *Ultrasonics Sonochemistry*, Vol. 55,(2019)
- [12] L. Lamparter, M. Galic, Cellular membranes, a versatile adaptive composite material, *Frontiers in Cell and Developmental Biology*, Vol. 8,(2020)
- [13] N. Li, et al., Synovial membrane mesenchymal stem cells: past life, current situation, and application in bone and joint diseases, *Stem Cell Research & Therapy*, Vol. 11,(2020)
- [14] W. Yao, J. Ma, X. Huang, Numerical simulation of the human ear and the dynamic analysis of the middle ear sound transmission, *Journal of Instrumentation*, Vol. 8, Iss.06,(2013)
- [15] M. Ugarteburu, R.H. Withnell, L. Cardoso, A. Carriero, C.P. Richter, Mammalian middle ear mechanics: A review, *Frontiers in Bioengineering and Biotechnology*, Vol. 10,(2022)
- [16] L. Caminos, J. Garcia-Manrique, A. Lima-Rodriguez, A. Gonzalez-Herrera, Analysis of the mechanical properties of the human tympanic membrane and its influence on the dynamic behaviour of the human hearing system, *Applied Bionics and Biomechanics*, Vol. 2018, Iss.1,(2018)

- [17] C. Wu, Y. Chen, M. Al-Furjan, J. Ni, X. Yang, Free vibration model and theoretical solution of the tympanic membrane, *Computer Assisted Surgery*, Vol. 21, Iss.sup1,(2016)
- [18] C. Wu, J. Ni, X. Yang, J. Lang, Research on the Tympanic Membrane Free Vibration Model Based on Thin Plate Theory, *Journal of Mechanics in Medicine and Biology*, Vol. 17, Iss.05,(2017)
- [19] L.C. Lobato, S. Paul, J.A. Cordioli, Statistical analysis of the human middle ear mechanical properties, *The Journal of the Acoustical Society of America*, Vol. 151, Iss.3,(2022)
- [20] X. Zhang, R.Z. Gan, Dynamic properties of human tympanic membrane based on frequency-temperature superposition, *Annals of Biomedical Engineering*, Vol. 41,(2013)
- [21] M. Ahmadvand, P. Asadi, Free vibration analysis of flexible rectangular fluid tanks with a horizontal crack, *Applied Mathematical Modelling*, Vol. 91,(2021)
- [22] Y. Mochida, S. Ilanko, On the Rayleigh-Ritz Method, Gorman's Superposition Method, and the Exact Dynamic Stiffness Method for Vibration and Stability Analysis of Continuous Systems, *Thin-Walled Structures*, Vol. 161,(2021)
- [23] C. Ye, Y.Q. Wang, On the use of Chebyshev polynomials in the Rayleigh-Ritz method for vibration and buckling analyses of circular cylindrical three-dimensional graphene foam shells, *Mechanics Based Design of Structures and Machines*, Vol. 49, Iss.7,(2021)
- [24] D. Du, W. Sun, X. Yan, K. Xu, Free vibration analysis of rotating thin-walled cylindrical shells with hard coating based on Rayleigh-Ritz method, *Proc IMechE Part G: Journal of Aerospace Engineering*, Vol. 235, Iss.10,(2021)
- [25] S. Bao, J. Cao, S. Wang, Vibration analysis of nanorods by the Rayleigh-Ritz method and truncated Fourier series, *Results in Physics*, Vol. 12,(2019)
- [26] E. Njim, S. Bakhy, M. Al-Waily, Analytical and numerical free vibration analysis of porous functionally graded materials (FGPMs) sandwich plate using Rayleigh-Ritz method, *Archives of Materials Science and Engineering*, Vol. 110, Iss.1,(2021)
- [27] M. Hussain, et al., On mixing the Rayleigh-Ritz formulation with Hankel's function for vibration of fluid-filled functionally graded cylindrical shell, *Advances in Computational Design*, Vol. 5, Iss.4,(2020)